Science
AAAS

Genome-Wide RNAi Screen Identifies Letm1 as a Mitochondrial Ca 2+/H+ Antiporter

Dawei Jiang, *et al.*

Science **326**, 144 (2009);
DOI: 10.1126/science.1175145

22. R. Curtis, G. O'Connor, P. S. DiStefano, *Aging Cell* **5**, 119 (2006).
23. K. Z. Pan *et al.*, *Aging Cell* **6**, 111 (2007).
24. V. Mieulet *et al.*, *Am. J. Physiol. Cell Physiol.* **293**, C712 (2007).
25. D. A. Guertin, D. M. Sabatini, *Sci. Signal.* **2**, pe24 (2009).
26. B. B. Zhang, G. Zhou, C. Li, *Cell Metab.* **9**, 407 (2009).
27. G. R. Chang *et al.*, *J. Pharmacol. Sci.* **109**, 496 (2009).
28. V. N. Anisimov *et al.*, *Cell Cycle* **7**, 2769 (2008).
29. D. E. Harrison *et al.*, *Nature* **460**, 392 (2009).

30. Supported by a Wellcome Trust Functional Genomics award to J.M.T., L.P., D.G., and D.J.W.; a Wellcome Trust Strategic Award to J.M.T., L.P., D.G., and D.J.W.; and grants from the Medical Research Council, Research into Aging, and the Biological and Biotechnology Research Council to D.J.W.

Supporting Online Material
www.sciencemag.org/cgi/content/full/326/5949/140/DC1
Materials and Methods
Figs. S1 and S2
Tables S1 to S5
References

3 June 2009; accepted 24 August 2009
10.1126/science.1177221

Genome-Wide RNAi Screen Identifies Letm1 as a Mitochondrial Ca^{2+}/H^{+} Antiporter

Dawei Jiang, Linlin Zhao, David E. Clapham*

Mitochondria are integral components of cellular calcium (Ca^{2+}) signaling. Calcium stimulates mitochondrial adenosine 5′-triphosphate production, but can also initiate apoptosis. In turn, cytoplasmic Ca^{2+} concentrations are regulated by mitochondria. Although several transporter and ion-channel mechanisms have been measured in mitochondria, the molecules that govern Ca^{2+} movement across the inner mitochondrial membrane are unknown. We searched for genes that regulate mitochondrial Ca^{2+} and H^{+} concentrations using a genome-wide *Drosophila* RNA interference (RNAi) screen. The mammalian homolog of one *Drosophila* gene identified in the screen, *Letm1*, was found to specifically mediate coupled Ca^{2+}/H^{+} exchange. RNAi knockdown, overexpression, and liposome reconstitution of the purified Letm1 protein demonstrate that Letm1 is a mitochondrial Ca^{2+}/H^{+} antiporter.

Mitochondrial Ca^{2+} uptake across the inner mitochondrial membrane occurs via tightly regulated channels [e.g., MCU/MiCa (*1*, *2*) and transporters (*3*–*6*)]. Increases in the concentration of calcium ($[Ca^{2+}]$) in the mitochondrial matrix enhance the activities of adenosine 5′-triphosphate (ATP) synthase and enzymes in the tricarboxylic acid cycle (*7*, *8*), but if homeostatic mechanisms fail, high levels of matrix Ca^{2+} induce cell death (*9*, *10*). We set out to identify the genes that mediate Ca^{2+} flux across the inner mitochondrial membrane.

We conducted a genome-wide, high-throughput RNA interference (RNAi) screen to identify genes that control mitochondrial Ca^{2+} transport. *Drosophila* S2 cells stably expressing mitochondria-targeted ratiometric pericam were incubated with arrayed double-stranded RNAs (dsRNAs) against each of the ~22,000 *Drosophila* genes (*11*). Mitochondrial (Mt)-pericam emission due to excitation at 405 nm is sensitive to changes in $[Ca^{2+}]$, whereas emission in response to excitation at 488 nm independently reports changes in pH (figs. S1 and S2). Through a series of screens discussed in the supporting online material (SOM) (fig. S2 and tables S1 to S3), *CG4589*, the *Drosophila* homolog of the human gene *Letm1*, was identified as a gene strongly affecting $[Ca^{2+}]_{mito}$ and $[H^{+}]_{mito}$

Department of Cardiology, Howard Hughes Medical Institute, Children's Hospital Boston, Manton Center for Orphan Disease, and Department of Neurobiology, Harvard Medical School, Enders Building 1309, 320 Longwood Avenue, Boston, MA 02115, USA.

*To whom correspondence should be addressed. E-mail: dclapham@enders.tch.harvard.edu

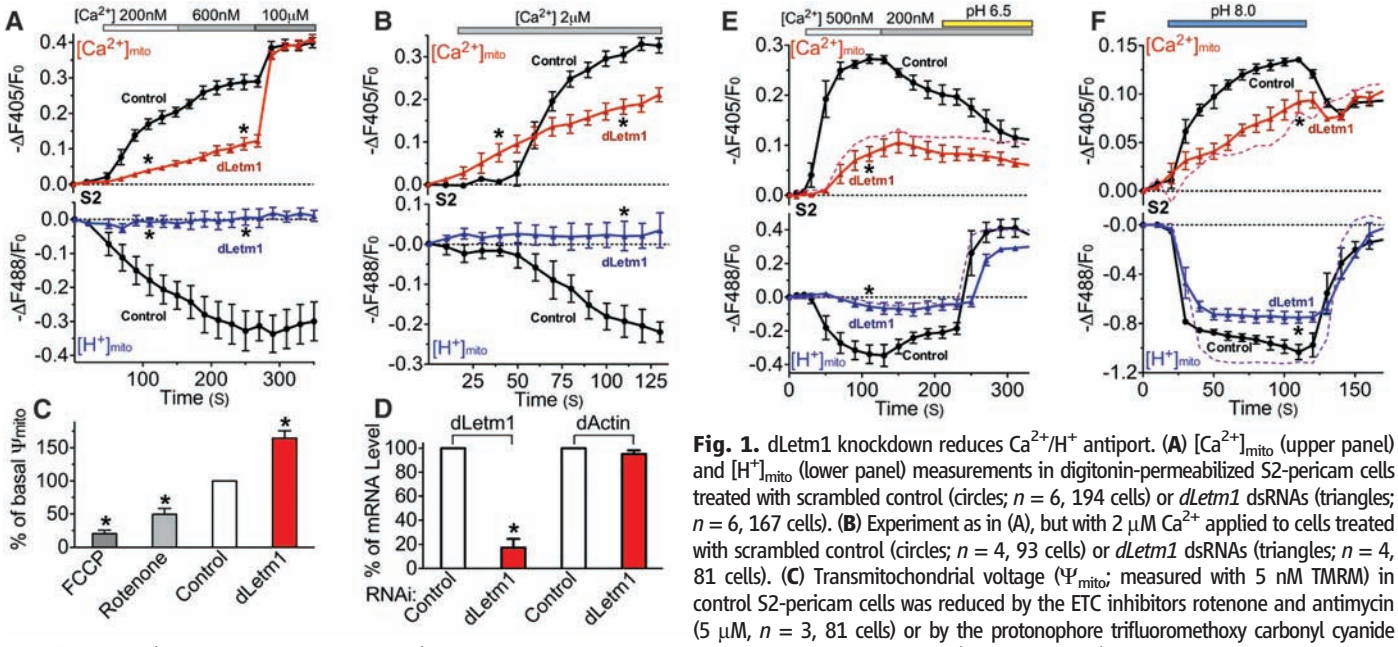

Fig. 1. dLetm1 knockdown reduces Ca^{2+}/H^{+} antiport. (**A**) $[Ca^{2+}]_{mito}$ (upper panel) and $[H^{+}]_{mito}$ (lower panel) measurements in digitonin-permeabilized S2-pericam cells treated with scrambled control (circles; $n = 6$, 194 cells) or *dLetm1* dsRNAs (triangles; $n = 6$, 167 cells). (**B**) Experiment as in (A), but with 2 μM Ca^{2+} applied to cells treated with scrambled control (circles; $n = 4$, 93 cells) or *dLetm1* dsRNAs (triangles; $n = 4$, 81 cells). (**C**) Transmitochondrial voltage (Ψ_{mito}; measured with 5 nM TMRM) in control S2-pericam cells was reduced by the ETC inhibitors rotenone and antimycin (5 μM, $n = 3$, 81 cells) or by the protonophore trifluoromethoxy carbonyl cyanide phenylhydrazone (FCCP; 10 μM, $n = 3$, 102 cells). By contrast, Ψ_{mito} was increased in dLetm1 knockdown cells ($n = 3$, 113 cells) as compared to cells treated with scrambled control dsRNA ($n = 3$, 168 cells). (**D**) Relative mRNA level of dLetm1 and actin in control and *dLetm1* dsRNA-treated S2 cells by quantitative reverse transcription–polymerase chain reaction (RT-PCR) ($n = 3$). (**E**) Ca^{2+}- and pH gradient–driven $[Ca^{2+}]_{mito}$ and $[H^{+}]_{mito}$ changes in permeabilized S2-pericam cells treated with control (circles; $n = 4$, 143 cells) or *dLetm1* dsRNAs (triangles; $n = 4$, 113 cells). A representative trace shows the effect of applying the H^{+}/K^{+} antiporter nigericin (1 μM, dashed colored line) on *dLetm1* dsRNA-treated cells ($n = 3$, 87 cells). (**F**) pH-dependent $[Ca^{2+}]_{mito}$ and $[H^{+}]_{mito}$ changes in permeabilized S2-pericam cells treated with scrambled control (circles; $n = 6$, 214 cells) or *dLetm1* dsRNAs (triangles; $n = 6$, 187 cells). BAPTA-maintained test solution $[Ca^{2+}] = 50$ nM. A representative trace shows the effect of nigericin (1 μM, dotted line) on *dLetm1* dsRNA-treated cells ($n = 3$, 104 cells). All data shown are the mean ± SEM (*$P < 0.05$, two-tailed Student's *t* test).

responses. Mammalian uncoupling proteins (UCPs) were recently proposed to be critical for Ca^{2+}_{mito} uptake (*12*) [but see (*13*)]. However, dsRNAs against *Drosophila* mitochondrial UCPs did not affect $[Ca^{2+}]_{mito}$ and $[H^+]_{mito}$ changes in our screen and subsequent assays (fig. S4).

Extramitochondrial $[Ca^{2+}]$ was clamped in permeabilized S2 cells in Na^+-free intracellular solution to abrogate potential mitochondrial Na^+ ($/H^+$ or $/Ca^{2+}$) exchangers. Basal $[Ca^{2+}]_{mito}$ and $[H^+]_{mito}$ were similar in control and dLetm1 knockdown cells under this condition (fig. S5). dLetm1 knockdown markedly reduced Ca^{2+}_{mito} uptake at <1 μM $[Ca^{2+}]_{cyto}$, a transport mode coupled with mitochondrial H^+ extrusion (Fig. 1A). Free $[Ca^{2+}]_{mito}$ at steady state was ~5 μM, far below the calculated free $[Ca^{2+}]_{mito}$ equilibrium (~1 M, assuming 1 μM cytoplasmic $[Ca^{2+}]$), indicating an intrinsic limit for this mode of uptake. At $[Ca^{2+}]_{cyto}$ >1 μM, a dLetm1-independent Ca^{2+}_{mito} uptake mode became apparent (Fig. 1B). This rapid Ca^{2+}_{mito} uptake mode stimulated by higher $[Ca^{2+}]_{cyto}$ was not associated with H^+_{mito} extrusion and caused membrane depolarization, consistent with MCU/MiCa. dLetm1 knockdown had little effect on 100 μM $[Ca^{2+}]_{cyto}$-induced Ca^{2+}_{mito} influx (Fig. 1A).

Ca^{2+}_{mito} uptake in cells lacking dLetm1 was not coupled with H^+_{mito} extrusion. We measured voltage across the inner mitochondrial membrane (Ψ_{mito}) using tetramethyl rhodamine methyl ester (TMRM; 5 nM) to determine whether dLetm1 knockdown affected electron transport chain (ETC)–dependent proton export. Unlike ETC inhibitors that reduce Ψ_{mito} in control cells, resting Ψ_{mito} was increased in dLetm1-knockdown cells (Fig. 1, C and D). To summarize the results thus far, dLetm1 is crucial to Ca^{2+}_{mito} uptake in low $[Ca^{2+}]$, and the pH gradient appears to intrinsically limit dLetm1-associated mitochondrial Ca^{2+} uptake.

To test the apparent limitation by the pH gradient, we studied pH-dependent changes on $[Ca^{2+}]_{mito}$ and $[H^+]_{mito}$. Ca^{2+}_{mito} extrusion and H^+_{mito} influx were induced by a decline in $[Ca^{2+}]_{cyto}$, and by cytoplasmic acidification (Fig. 1E). dLetm1 knockdown specifically abolished Ca^{2+}-dependent pH changes and pH-driven Ca^{2+}_{mito} extrusion. As expected, alkalinization induced an initial phase of rapid Ca^{2+}_{mito} uptake and H^+_{mito} extrusion, and a much slower second phase of Ca^{2+}_{mito} uptake and H^+_{mito} extrusion (Fig. 1F). The pH-dependent Ca^{2+}_{mito} uptake was slowed by more than fourfold in dLetm1 knockdown cells. In the yeast *mdm38* (homolog of *Letm1* and *CG4589*) mutant, mitochondria were swollen and the phenotype could be rescued

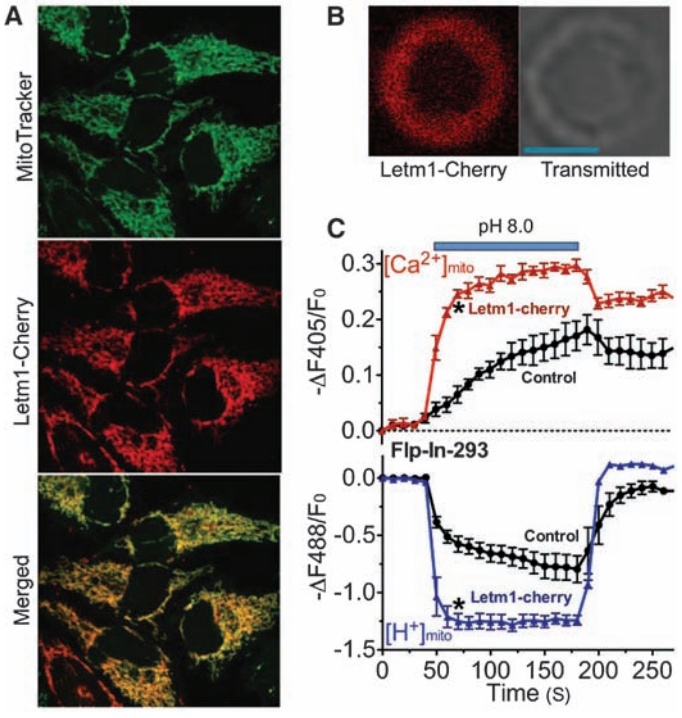

Fig. 2. Letm1 overexpression enhances Ca^{2+}/H^+ antiport. (**A**) Letm1 is localized to mitochondria. Representative images of Flp-In-293-pericam cells transfected with Letm1-Cherry and loaded with 10 nM MitoTracker green. (**B**) Representative image of a Letm1-Cherry–labeled mitoplast; Letm1-Cherry was targeted to the mitochondrial inner membrane. Scale bar: 2 μm. (**C**) Alkaline pH (pH 8.0) increased $[Ca^{2+}]_{mito}$ and decreased $[H^+]_{mito}$ in digitonin-permeabilized Flp-In-293-pericam cells in vector controls (circles; n = 5, 119 cells). Overexpression of Letm1-Cherry (triangles; n = 5, 93 cells) enhanced these changes. $[Ca^{2+}]_o$ = 250 nM. Data shown are the mean ± SEM (*P < 0.05, two-tailed Student's t test).

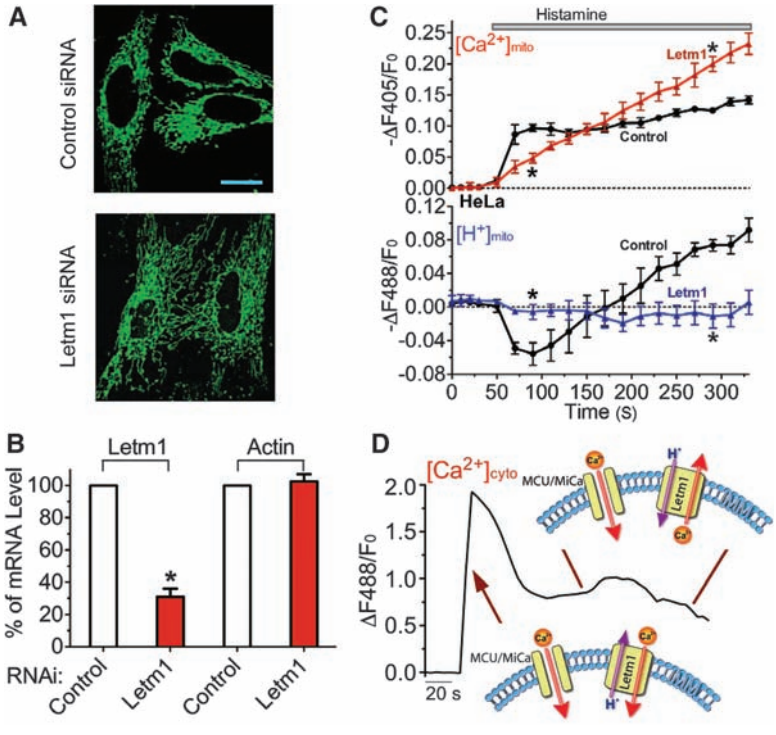

Fig. 3. Letm1 knockdown disrupts Ca^{2+}/H^+ antiport in intact cells. (**A**) mt-Pericam–labeled mitochondria appear grossly normal in a representative image of *Letm1* siRNA-treated HeLa cells compared to cells treated with scrambled control siRNA. Scale bar: 20 μm. (**B**) Determination of the mRNA level of Letm1 and actin in control and *Letm1* siRNA-treated HeLa cells by quantitative RT-PCR (n = 3). (**C**) Letm1 knockdown disturbs normal mitochondrial $[Ca^{2+}]_{mito}$ and $[H^+]_{mito}$ regulation in H1R-expressing HeLa cells. Histamine was applied to stimulate an increase in cytoplasmic $[Ca^{2+}]$ in cells in $[Ca^{2+}]_o$ = 2 mM treated with control (circles; n = 8, 76 cells) or *Letm1* siRNAs (triangles; n = 6, 47 cells). Two independent *Letm1* siRNAs were used to confirm the result. (**D**) Representative trace of the $[Ca^{2+}]_{cyto}$ changes in HeLa cells upon histamine stimulation, and model of the roles of MCU/MiCa and Letm1 Ca^{2+}/H^+ exchanger activity under these conditions (arrows indicate their actions during the trace). All data shown are the mean ± SEM (*P < 0.05, two-tailed Student's t test).

by the exogenous K^+/H^+ exchanger, nigericin (*14*). In these studies, however, active mitochondrial K^+/H^+ exchange was only observed under low-divalent or divalent-free conditions (*14*). In our experiments in dLetm1 knockdown S2 cells, application of nigericin augmented H^+ flux (Fig. 1, E and F), but did not rescue the loss of pH-driven Ca^{2+} exchange.

The human homolog of *CG4589*, *Letm1* (leucine zipper EF-hand–containing transmembrane protein 1), is an evolutionarily conserved, ubiquitously expressed, homomeric inner mitochondrial membrane protein of unclear function (*15*–*18*). In humans, partial deletion of the short arm of chromosome 4 (including *Letm1*) results in Wolf-Hirschhorn syndrome (WHS), characterized by mental retardation, microcephaly, seizures, hypotonia, and cleft lip/palate (*19*). In mammalian cells, Cherry-tagged Letm1 was exclusively localized to the mitochondrial inner membrane (Fig. 2, A and B). In cells overexpressing Letm1, pH-driven Ca^{2+}_{mito} uptake and H^+_{mito} extrusion were accelerated by more than fivefold (Fig. 2C). Mitochondrial H^+ transport was not secondary to $[Ca^{2+}]_{mito}$ alone, but rather to the Ca^{2+} gradient across the inner mitochondrial membrane (fig. S6).

Most HeLa cells with short-term (~3 days) *Letm1* small interfering RNA (siRNA) treatment appeared healthy and their mitochondria appeared normal under light microscopy (Fig. 3A), despite an ~70% reduction in mRNA level (Fig. 3B). Knockdown of Letm1 abolished bidirectional mitochondrial Ca^{2+}/H^+ antiport, resulting in reduced initial Ca^{2+}_{mito} uptake and late Ca^{2+}_{mito} overload (Fig. 3, C and D), supporting the essential role of Letm1 in Ca^{2+}/H^+ antiporter function and $[Ca^{2+}]_{mito}$ homeostasis. As in S2 cells, knockdown of Letm1 did not cause a decrease, but rather a slight increase, in resting Ψ_{mito} (fig. S7), consistent with a previous report that Letm1 knockdown does not impair ETC function (*17*).

To directly test whether the Letm1 protein mediates Ca^{2+}/H^+ antiport, C-terminal His-tagged Letm1 was expressed in bacteria, purified (Fig. 4A), and incorporated into liposomes. Letm1-containing liposomes rapidly accumulated Ca^{2+}. Ca^{2+} uptake was blocked by Ruthenium red (and Ru360), nonselective inhibitors of divalent cation channels and transporters (Fig. 4B). CGP-37157 (~4 μM), a nonselective inhibitor of Na^+/Ca^{2+} exchangers, inhibited the transport rate by ~25%. Addition of Ca^{2+} induced H^+ efflux; also transiently increasing external pH induced rapid H^+ efflux from Letm1-liposomes (Fig. 4C). In symmetrical $[Ca^{2+}]$, external acidic pH drove Ca^{2+} release (Fig. 4D), whereas alkaline pH induced Ca^{2+} uptake (Fig. 4E). The maximum rate of Ca^{2+} transport (V_{max}) by isolated Letm1 protein was 4.1 nmol/μg protein per second [~1700 ions per second, assuming that Letm1 is tetrameric (*22*, *23*)], reaching half-saturation at 132.7 nmol Ca^{2+}/μg protein; Michaelis constant (K_m) = 137 nmol Ca^{2+}/μg protein (Fig. 4F). Ca^{2+} transport velocity was increased about sevenfold by increasing the transliposomal potential (fig. S8), suggesting that Letm1 is electrogenic. These results, using isolated Letm1-containing liposomes, strongly suggest that Letm1 itself comprises a Ca^{2+}/H^+ antiporter.

We showed that Letm1 is a Ca^{2+}/H^+ exchanger in S2 cells, mammalian cells, and as an isolated protein in proteoliposomes. Letm1 exchanges Ca^{2+} for H^+ at submicromolar $[Ca^{2+}]_{cyto}$. When $[Ca^{2+}]_{mito}$ is high, such as after MCU/MiCa activation, or when cytoplasmic pH is low, Letm1 should extrude excess Ca^{2+} and acidify the mitochondrial matrix. When $[Ca^{2+}]_{mito}$ is low, Ca^{2+} will be imported and the mitochondrial matrix alkalinized. Letm1 Ca^{2+}/H^+ exchange was not sensitive to $[Na^+]$. Prior evidence for Na^+-dependent Ca^{2+} extrusion suggests that a third molecule, probably a Na^+/Ca^{2+} exchanger, is also present in the inner mitochondrial membrane (*1*, *4*, *5*). We speculate that the relative amounts of these three Ca^{2+}-exchange mechanisms vary in different cell types, correlating with their cell-specific functions.

We found that long-term Letm1 knockdown with repetitive siRNA application resulted in morphological changes in certain HeLa cell subpopulations (~20% cells). However, other studies showed no mitochondrial morphology changes in lymphoblastoid cells and primary fibroblasts from WHS patients despite a notable reduction in the amount of Letm1 protein (*17*). These data suggest that mitochondrial morphology changes

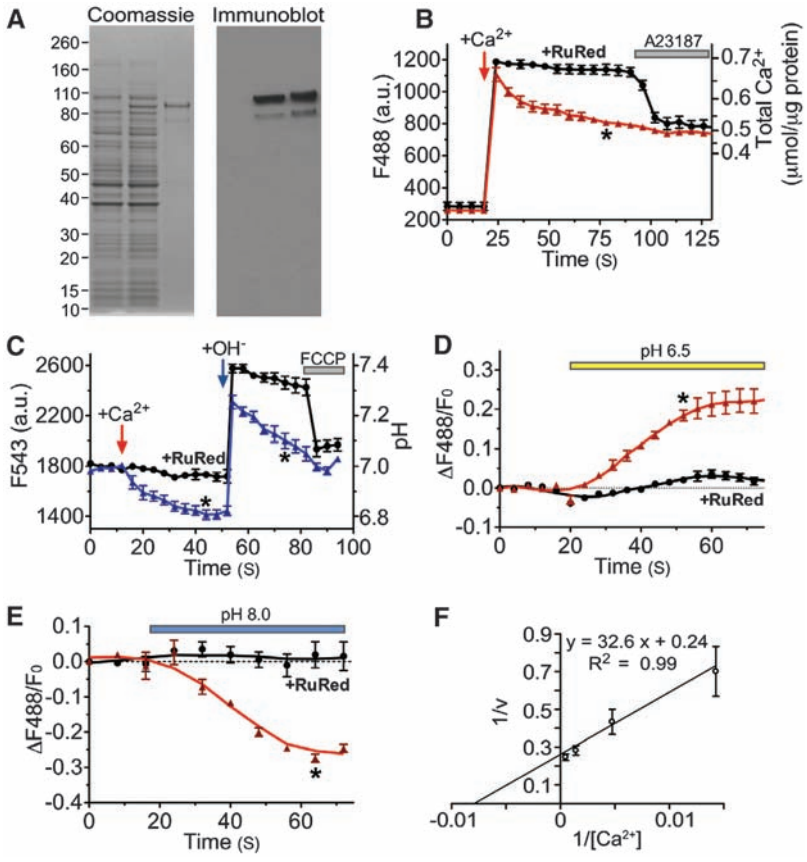

Fig. 4. Purified Letm1 reconstitutes Ca^{2+} transport in liposomes. (**A**) Letm1 protein stained by Coomassie blue (left) and antibody to His-Letm1 (right). Left lane, total bacterial cell lysate from control; middle lanes, Letm1-His–expressing bacteria; right lanes, isolated Letm1-His proteins. The band migrating at ~83 kD is consistent with Letm1's predicted molecular size. (**B**) Ca^{2+} addition initially increased external Ca^{2+}, followed by Ca^{2+} import as indicated by decreasing fluorescence (triangles; n = 8). Ca^{2+} uptake was blocked by Ruthenium red (RuR; 10 nmol/μg; circles; n = 5), which was reversed by the Ca^{2+} ionophore, A23187 (5 μM). Liposomes occupied ~30% of the total volume based on the maximum Ca^{2+} uptake triggered by 4-Bromo-A23187. No leak was detected in liposomes without Letm1. (**C**) Ca^{2+}-driven H^+ efflux in Letm1 proteoliposomes. Addition of 100 μM Ca^{2+} triggered H^+ efflux; application of 100 μM CsOH transiently increased the external pH, followed by a rapid decline in pH (triangles; n = 5), which was blocked by RuR (10 nmol/μg; circles; n = 3). Finally, FCCP (10 μM, protonophore) reduced the external pH to basal levels. (**D** and **E**) pH-driven Ca^{2+} uptake in Letm1 proteoliposomes; Ca^{2+} release or uptake in Letm1 proteoliposomes was blocked by RuR. No-added-RuR, triangles, n = 4; 10 nmol/μg RuR, circles, n = 3. (**F**) The inverse Ca^{2+} transport velocity (1/v; nmol/μg protein per second) was plotted against inverse total added $[Ca^{2+}]$ (nmol/μg protein, n = 3 to 8) in this double reciprocal plot to calculate K_m (137 nmol Ca^{2+}/μg protein) and V_{max} (4.2 nmol/μg protein per second) using Michaelis-Menten assumptions (*24*). All data shown are the mean ± SEM (*P < 0.05 in a two-tailed Student's t test).

are secondary to the loss of Letm1, but may depend on cell type.

Letm1 has no appreciable homology to the bacterial and plant CaX family of Ca^{2+}/H^{+} or Ca^{2+}/Na^{+} transporters. Based on our preliminary analysis of the potential topologies using *Robetta* (fig. S9) (*20*), we hypothesize that Letm1 resembles the inner mitochondrial membrane Mg^{2+} transporter (*21*), whose bacterial homolog (CorA) forms a funnel-shaped structure (*22*, *23*).

References and Notes

1. R. Rizzuto, P. Bernardi, T. Pozzan, *J. Physiol.* **529**, 37 (2000).
2. Y. Kirichok, G. Krapivinsky, D. E. Clapham, *Nature* **427**, 360 (2004).
3. K. K. Gunter, T. E. Gunter, *J. Bioenerg. Biomembr.* **26**, 471 (1994).
4. P. Bernardi, *Physiol. Rev.* **79**, 1127 (1999).
5. N. Demaurex, D. Poburko, M. Frieden, *Biochim. Biophys. Acta* **1787**, 1383 (2009).
6. D. G. Nicholls, *Biochim. Biophys. Acta* **1777**, 550 (2008).
7. G. Szabadkai, M. R. Duchen, *Physiology (Bethesda)* **23**, 84 (2008).
8. G. Hajnoczky, L. D. Robb-Gaspers, M. B. Seitz, A. P. Thomas, *Cell* **82**, 415 (1995).
9. A. Rasola, P. Bernardi, *Apoptosis* **12**, 815 (2007).
10. M. Giacomello, I. Drago, P. Pizzo, T. Pozzan, *Cell Death Differ.* **14**, 1267 (2007).
11. N. Ramadan, I. Flockhart, M. Booker, N. Perrimon, B. Mathey-Prevot, *Nat. Protocols* **2**, 2245 (2007).
12. M. Trenker, R. Malli, I. Fertschai, S. Levak-Frank, W. F. Graier, *Nat. Cell Biol.* **9**, 445 (2007).
13. P. S. Brookes *et al.*, *Nat. Cell Biol.* **10**, 1235 (2008).
14. K. Nowikovsky, S. Reipert, R. J. Devenish, R. J. Schweyen, *Cell Death Differ.* **14**, 1647 (2007).
15. L. Piao *et al.*, *Cancer Res.* **69**, 3397 (2009).
16. S. Tamai *et al.*, *J. Cell Sci.* **121**, 2588 (2008).
17. K. S. Dimmer *et al.*, *Hum. Mol. Genet.* **17**, 201 (2008).
18. A. Hasegawa, A. M. van der Bliek, *Hum. Mol. Genet.* **16**, 2061 (2007).
19. A. D. Bergemann, F. Cole, K. Hirschhorn, *Trends Genet.* **21**, 188 (2005).
20. D. E. Kim, D. Chivian, D. Baker, *Nucleic Acids Res.* **32**, W526 (2004).
21. R. Schindl, J. Weghuber, C. Romanin, R. J. Schweyen, *Biophys. J.* **93**, 3872 (2007).
22. V. V. Lunin *et al.*, *Nature* **440**, 833 (2006).
23. S. Eshaghi *et al.*, *Science* **313**, 354 (2006).
24. Materials and methods and references are given in the supporting material available on *Science* Online.

25. We thank B. Mathey-Prevot, N. Ramadan, M. Booker, and staff at the Drosophila RNAi Screening Center for assistance with the screen; A. Miyawaki for pericam; R. Tsien for CherryFP; T. Schwarz for the PMK33 vector; R. Kaplan for advice on the proteoliposome study; D. Baker for assistance with *Robetta*; and G. Krapivinsky, Y. Kirichok, and J. Jin for discussions. D.J. is a recipient of fellowship awards from the Canadian Institutes of Health Research and the Alberta Heritage Foundation for Medical Research.

Supporting Online Material

www.sciencemag.org/cgi/content/full/326/5949/144/DC1
SOM Text
Materials and Methods
Figs. S1 to S9
Tables S1 to S3

20 April 2009; accepted 4 August 2009
10.1126/science.1175145

Dissecting the Genetic Basis of Resistance to Malaria Parasites in *Anopheles gambiae*

Stephanie A. Blandin,[1,2]* Rui Wang-Sattler,[1,3]* Marina Lamacchia,[2] Julien Gagneur,[1] Gareth Lycett,[1]† Ye Ning,[1]‡ Elena A. Levashina,[2] Lars M. Steinmetz[1]§

The ability of *Anopheles gambiae* mosquitoes to transmit *Plasmodium* parasites is highly variable between individuals. However, the genetic basis of this variability has remained unknown. We combined genome-wide mapping and reciprocal allele-specific RNA interference (rasRNAi) to identify the genomic locus that confers resistance to malaria parasites and demonstrated that polymorphisms in a single gene encoding the antiparasitic thioester-containing protein 1 (TEP1) explain a substantial part of the variability in parasite killing. The link between *TEP1* alleles and resistance to malaria may offer new tools for controlling malaria transmission. The successful application of rasRNAi in *Anopheles* suggests that it could also be applied to other organisms where RNAi is feasible to dissect complex phenotypes to the level of individual quantitative trait alleles.

Anopheles gambiae mosquitoes are major vectors of *Plasmodium falciparum*, a protozoan parasite that causes the most severe form of human malaria in Africa. The fact that mosquito strains that are completely resistant to malaria parasites can be selected (*1*, *2*) indicates that genetic factors in mosquitoes control the level of parasite transmission. Understanding the genetic basis of this resistance has been a long-standing question. The L3-5 resistant strain kills and melanizes a wide variety of parasite species (*1*). Previous genetic analyses of crosses between this strain and the susceptible 4Arr strain infected with two simian parasite species focused on the melanotic encapsulation phenotype and identified several quantitative trait loci (QTLs), whose relative contributions varied with parasite species and between F2 generation families (*3*, *4*). Recently, it became clear that melanization occurs after parasite killing as a means to dispose of dead parasites in some strains, whereas in others, killed parasites are only cleared by lysis (fig. S2A) (*5*–*7*). In this study, we aimed at mapping the genomic regions and identifying genes that control resistance (the absence of live parasites) of mosquitoes to the rodent malaria parasite *Plasmodium berghei*.

We set up reciprocal crosses of the resistant L3-5 and susceptible 4Arr strains. F1 mosquitoes were intercrossed, and individual females were isolated to lay eggs, yielding 10 F2 families. Females were blood-fed on mice infected with *PbGFPcon*, a transgenic clone of *P. berghei* expressing *GFP* constitutively (*8*). Fluorescent live and dead melanized parasites were counted on dissected midguts 7 to 9 days post infection [Fig. 1A and supporting online material (SOM) text]. As expected, parental L3-5 females displayed only melanized parasites (with the exception of one that bore one live parasite), and 4Arr mosquitoes displayed only live parasites. Most of the 111 F1 mosquitoes exhibited an intermediate phenotype (mix of live and melanized parasites). Both parental and F1 phenotypes were present in the 402 F2 females. Percentages of resistant (devoid of live parasite) and melanizing (bearing at least one melanized parasite) mosquitoes in each generation (Fig. 1B) did not follow the segregation pattern of simple Mendelian traits [$P < 0.001$ in both cases (*9*)], indicating that the killing of *P. berghei* and the mode of clearance of dead parasites are complex traits that are each likely to result from the segregation of several alleles.

To map loci controlling resistance to parasites, we genotyped 39 informative markers spanning the entire genome in 206 selected F2 individuals with extreme phenotypes (fig. S1 and SOM text). Linkage analysis comparing resistant and nonresistant mosquitoes identified a single region on chromosome 3L (Fig. 1C). We interpreted this region, covering ~19 Mb, as a major locus responsible for resistance to *P. berghei* and named it *Pbres1* for *P. berghei* resistance locus 1. We further compared the genotypes of melanizing and nonmelanizing mosquitoes and detected two intervals that are likely to contain regulators affecting the mode of clearance of dead parasites (i.e., the balance between lysis and melanization) (Fig. 1C): (i) a major QTL on chromosome 2R, which we named *Pbmel1* (5 Mb) for *P. berghei* melanization locus 1, and (ii) a minor pericentromeric QTL on chromosome 3, *Pbmel2* (17 Mb), that partially overlaps with *Pbres1*. Linkage map-

[1]European Molecular Biology Laboratory (EMBL), Meyerhofstrasse 1, 69117 Heidelberg, Germany. [2]CNRS UPR9022, INSERM U963, 15 rue Descartes, 67084 Strasbourg, France. [3]Institute of Epidemiology, Helmholtz Zentrum München, Ingolstädter Landstrasse 1, 85764 Munich/Neuherberg, Germany.

*These authors contributed equally to this work.
†Present address: Liverpool School of Tropical Medicine, Pembroke Place, Liverpool, L3 5QA, UK.
‡Present address: Faculty of Life Sciences, University of Copenhagen, Thorvaldsensvej 40, 1870 Frederiksberg C, Denmark.
§To whom correspondence should be addressed. E-mail: larsms@embl.de